# Systematic Control of Monoclinic $CdWO_4$ Nanophase for Optimum Photocatalytic Activity

**Wenming Tong,[†,‡] Liping Li,[†] Wanbiao Hu,[†] Tingjiang Yan,[†] and Guangshe Li*[,†]**

*State Key Lab of Structural Chemistry, Fujian Institute of Research on the Structure of Matter, Chinese Academy of Sciences, Fuzhou 350002, and School of Chemistry and Chemical Engineering, Inner Mongolia University, Hohhot 010021, People's Republic of China*

*Received: October 27, 2009; Revised Manuscript Received: December 13, 2009*

$CdWO_4$ nanocrystals with controlled particle size and crystallinity were successfully synthesized via a simple hydrothermal method using citric acid as the capping agent. By systematic sample characterization using X-ray powder diffraction, transmission electron microscope, selected area electron diffraction, Barret−Emmett−Teller technique, Fourier transformed infrared spectra, UV−visible diffuse reflectance spectra, and photoluminescence spectra, all as-prepared $CdWO_4$ samples were demonstrated to crystallize in a pure-phase of monoclinic wolframite structure. With varying the reaction temperature from 160 to 220 °C, particle size was controlled to grow from 11 to 21 nm. With particle size reduction, $CdWO_4$ nanostructure showed a lattice expansion, as is followed by a surprisingly lowered lattice symmetry, band gap broadening, and red-shift of $A_u$ vibration mode. Photocatalytic activity of $CdWO_4$ nanocrystals was examined by monitoring the degradation of methyl orange dye in an aqueous solution under UV radiation of 254 nm. High crystallinity $CdWO_4$ nanostructures with relatively small particle size showed an optimum photocatalytic performance. Consequently, systematic control over semiconductor nanostructures is proved to be useful, in some cases likely general, in achieving the advanced photocatalytic properties for technological uses.

## 1. Introduction

Exploring novel semiconductors of photocatalytic activity has received great attention because of the merits in degradation of organic pollutant in water or air, necessary for resolving many environmental pollution problems that mankind is facing nowadays.[1] Depending on the types and activities of semiconductors, photocatalytic reactions can work at ambient conditions, producing nontoxic $CO_2$ and water without generating any additional pollutant substances.[2]

It is well-known that the photocatalytic activity of semiconductors is strongly determined by several microstructural factors such as particle size, surface chemistry, morphology, and crystallinity. Among these factors, two contradictory aspects of almost all nanostructures, small particle size and high crystallinity, could be most important, since small particle size may give rise to large surface area and moreover significant amounts of active sites, while crystallinity directly determines the lattice perfection and moreover the electronic structures for activities.[3] When absorbing a photon with energy higher than or equal to the band gap energy, electrons in semiconductors can be excited from the filled valence band to the empty conduction band, leaving a "hole" in the valence band. These separated electrons and holes can induce an efficient photodegradation of organic pollutants, since the conduction band electrons can interact with the dissolving oxygen to generate highly reactive superoxide radicals to oxidize many organic compounds, while the holes can oxidize the organic pollutant by reacting with $H_2O$ or $OH^-$ on the surface of photocatalysis to produce a powerful oxidant such as hydroxyl radicals.[4] The recombination rate of the electron and hole may thus have a great impact on the photodegradation efficiency. Since the recombination of electrons and holes readily occurs at lattice defects, small particle size and high crystallinity that govern the solid defects should be the key for excellent photocatalytic activity of semiconductors.[3a,b,4c]

There are two approaches that are frequently used to enhance the crystallinity of semiconductors: prolonging the reaction time or increasing the reaction temperature. Nevertheless, both approaches will also result in a significant grain growth, which in turn reduces the surface area and furthermore decreases the photocatalytic activity due to the reduced active site numbers and photonic efficiency.[4d,5] How to prepare semiconductors that simultaneously possess two contradictory features of high crystallinity and smaller particle size is a challenge to achieve excellent photocatalytic performance.

We anticipate that it is highly possible to synthesize small particle-sized semiconductors of high crystallinity via a size-controlled synthesis using citric acid as the capping agent, since capping molecules of citric acid can effectively adjust the relative activity of the cation and moreover retard the grain growth of semiconductors.[6] For this purpose, the wide-gap semiconductor $CdWO_4$ was taken as a model compound to study. $CdWO_4$ represents a very relevant class of semiconductors because of its applications in many fields including phosphors, laser crystals, and catalysis. $CdWO_4$ crystallized in a monoclinic wolframite structure with a relatively high chemical stability.[7] Recently, Ye et al.[8] investigated the photocatalytic property of monoclinic $CdWO_4$ by UV light photodegradation of MO and found that $CdWO_4$ exhibits photocatalytic activity comparable to the known semiconductors $ZnWO_4$ and $TiO_2$. Nevertheless, the particle size reported for $CdWO_4$ nanostructures in literature[9] is always lack of control, which makes it very difficult to understand the impacts of the crystallinity and particle sizes on the photocatalytic activity.

In this work, we report on a systematic control over the $CdWO_4$ nanostructure for optimum photocatalytic activities.

* To whom correspondence should be addressed. Phone: +86-591-83702122. Fax: +86-591-83714946. E-mail: guangshe@fjirsm.ac.cn.
† Chinese Academy of Sciences.
‡ Inner Mongolia University.

10.1021/jp910284u 
Published on Web 01/04/2010

$CdWO_4$ nanocrystals with different size and crystallinity were hydrothermally synthesized using citric acid as the capping molecule. Our preliminary experimental results showed that both crystallinity and small particle sizes of $CdWO_4$ nanocrystals could be balanced to show optimum photocatalytic activity.

## 2. Experimental Section

**2.1. Sample Preparation.** Different particle sizes of $CdWO_4$ nanocrystals were synthesized by simple hydrothermal method. All chemicals were analytical grade and used without further purification. $CdCl_2 \cdot 2.5H_2O$ (2.96 g, 0.013 mol) and $C_6H_8O_7 \cdot H_2O$ (2.73 g, 0.013 mol) were dissolved into certain amounts of deionized water and then mixed with $Na_2WO_4 \cdot 2H_2O$ (4.29 g, 0.013 mol) to get a clear solution. A well-controlled NaOH solution was added into the clear solution with magnetic stirring until the pH value reached 8. This resulting mixture was transferred to a 100 mL Teflon-lined stainless steel autoclave that was allowed to react at given temperatures for 16 h and then cooled to room temperature naturally. The white products were centrifuged and washed with deionized water several times to remove all impurity species and then dried at 80 °C for 3 h.

**2.2. Sample Characterization.** Infrared spectra of the samples were measured on a Perkin-Elmer IR spectrophotometer at a resolution of 4 $cm^{-1}$ using KBr pellet technique. Photoluminescence (PL) properties of the samples were recorded on a Varian Cary Eclipse Fluorescence spectrophotometer. The sample structures were characterized by X-ray diffraction (XRD) on a Rigaku MiniFlex II benchtop X-ray diffractometer using a copper target. The average crystallite size, $D$, was calculated from the diffraction line (110) using the Scherrer formula, $D = 0.9\lambda/\beta\cos\theta$, where $\lambda$ is the X-ray wavelength employed, $\theta$ is the diffraction angle of the diffraction peak (110), and $\beta$ is defined as the half-width after the instrumental broadening is subtracted. The lattice parameters of the samples were calculated by a least-squares method using Rietica Rietveld software. Ni powder serves as an internal standard for peak position determination.

Particle size and morphology of the samples were determined using transmission electron microscope (TEM) on a JEM-2010 apparatus with an acceleration voltage of 200 kV. UV−vis diffuse reflectance spectra of the samples were recorded on a Varian Cary 500 scan UV−vis−NIR spectrophotometer with $BaSO_4$ as the background and in the range 200−800 nm. Specific surface areas of the samples were determined from the nitrogen absorption data at liquid nitrogen temperature using the Barrett−Emmett−Teller (BET) technique on a Micromeritics ASAP 2000 surface area and porosity analyzer.

**2.3. Photocatalytic Activity Test.** Methyl orange (MO) was used as a probe molecule to evaluate the photocatalytic activity of the samples in response to ultraviolet light at room temperature. MO is a water-soluble azo dye and is a water pollutant frequently produced in textile, paper manufacture, printing, pulp processing, and pharmaceutical industries.[10] All experiments were carried out as follows: 150 mg of the samples was dispersed in 150 mL of 10 ppm MO aqueous solution in a quartz tube with 4.6 cm inner diameter and 17 cm length. Prior to illumination, the suspensions were magnetically stirred in the dark for 3 h to ensure the establishment of absorption/desorption equilibrium of MO on the sample surfaces. Subsequently, the suspension was irradiated around by four UV lamps (4 W) with a wavelength centered at 254 nm (Philips, TUV 4W/G4 T5). A 3 mL aliquot was taken at given intervals and subsequently centrifuged at a rate of 6500 rpm for 15 min to remove the powders. UV−vis absorption spectra of the supernatant were then measured with a Perkin-Elmer UV lambda 35 spectrophotometer.

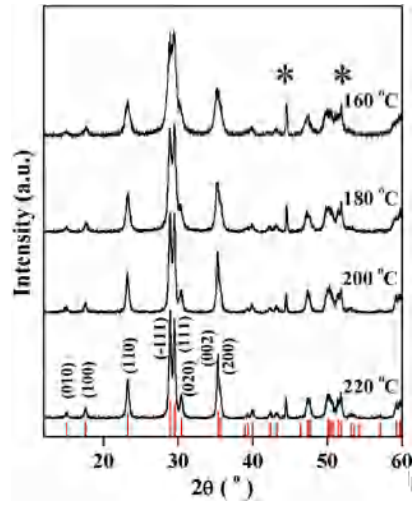


**Figure 1.** Selected XRD patterns of $CdWO_4$ prepared at different temperatures. Vertical bars represent the standard diffraction data for bulk $CdWO_4$. Bracketed numbers are the Miller indices for specific crystal faces. Symbol * represents the diffraction lines of internal standard nickel.

## 3. Results and Discussion

**3.1. Structure and Morphology of the Size-Controlled Monoclinic $CdWO_4$ Nanophases.** Figure 1 shows XRD patterns of the samples that were prepared at temperatures ranging from 160 to 220 °C. The standard diffraction data for bulk $CdWO_4$ (JCPDS, no. 14-0676) are also shown for comparison. It is seen that the diffraction peaks can be indexed as a monoclinic wolframite structure with no traces of impurities. With increasing the reaction temperature, XRD patterns became sharper, which indicates the increased crystallinity and grain growth as well. From the indexing results in Figure 1, the main peak (−111) is seen overlapped with (111) peak when the samples were prepared at lower temperatures. Particle sizes for the as-prepared samples were estimated from (110) peak broadening. When prepared at 160 °C, the particle size was as small as 11 nm. Increasing the reaction temperature to 220 °C led to an increase in particle size to 21 nm. These estimated particle sizes were approximately the same as those observed by TEM (Figure 2). Therefore, particle size of $CdWO_4$ nanocrystals could be effectively controlled in the presence of citric acid by varying the reaction temperature, which appears superior over the literature work.[8,9,11] For the latter cases, the synthesis of $CdWO_4$ nanoparticles is always lack of control, and the relevant particle sizes are usually larger ranging from tens of nanometers to hundreds of nanometers.

The successful control over the $CdWO_4$ nanostructures in this work might be benefited from the capping agent citric acid that was involved. When $CdCl_2$ and citric acid were dissolved into water, citric species might be easily chemically bonded to $Cd^{2+}$ to form the relatively stable coordination complexes. These stable coordination complexes could not release $Cd^{2+}$ into the reaction systems to react with $WO_4^{2-}$, and therefore, no $CdWO_4$ was formed at room temperature. Adding some amounts of NaOH can alter the activity of $WO_4^{2-}$ species and the coordination ability of $Cd^{2+}$ to citric species that may favor the formation of the $CdWO_4$ seeds. Consequently, $CdWO_4$ nanocrystals with controlled particle size and crystallinity were achieved by altering the reaction temperature.[6]

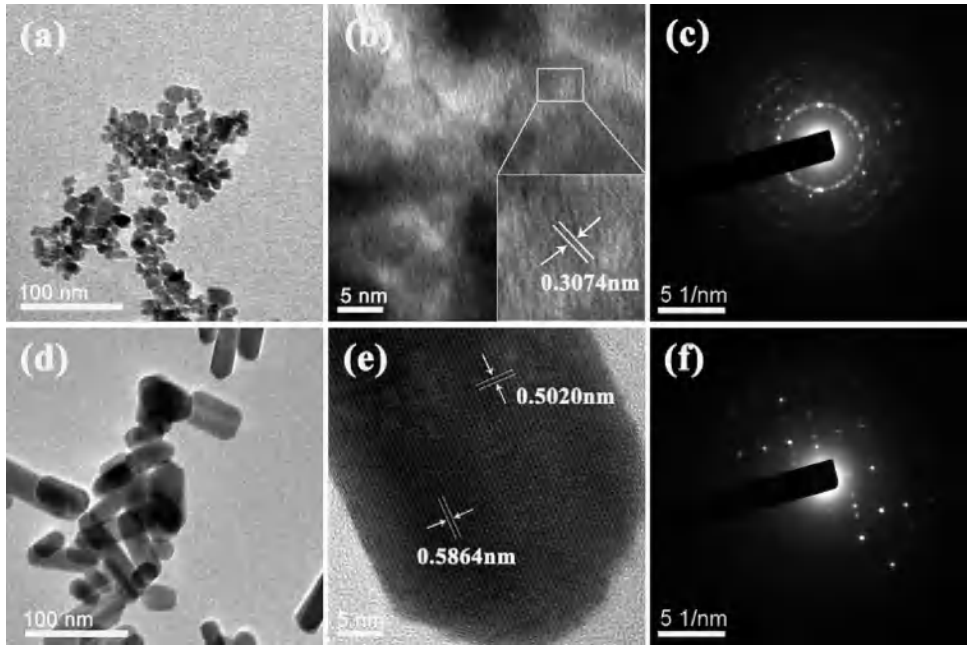


**Figure 2.** (a) TEM, (b) HRTEM, and (c) SAED images of 11 nm $CdWO_4$; (d) TEM, (e) HRTEM, and (f) SAED images of 21 nm $CdWO_4$.

Particle sizes and morphologies of $CdWO_4$ nanocrystals were determined by TEM observations. As indicated in Figure 2a and d, $CdWO_4$ nanocrystals prepared at 160 °C are an aggregate of tiny spindly-like particles with diameter of about 11 nm, consistent with XRD analysis. From the high-resolution TEM image (Figure 2b), the spacing between two adjacent lattice fringes was 0.3074 nm, compatible with that of 0.3077 nm for the $(\bar{1}11)$ plane by selected area electron diffraction (Figure 2c). When the formation reaction increased to 220 °C, particles grew up to 21 nm, showing a short rodlike shape. These rodlike particles are tiny single crystals, showing lattice plane spaces of 0.5020 and 0.5864 nm that can be indexed as (100) and (010) (Figure 2e). By comparative analysis of HRTEM and SAED images (Figure 2b, e, and f), 21 nm $CdWO_4$ was found to show a better crystallinity. Therefore, the increase in particle size is followed by an apparent crystallinity enhancement.

Closely related to the rodlike morphology is the aspect ratio, which is important in controlling the exciton transport rate and moreover the photocatalytic oxidation ability. As indicated in Figure 2d, the particles for 21 nm $CdWO_4$ are all larger and distributed in a broad range, which makes it difficult to precisely obtain the aspect ratio. Here, the diffraction intensity ratio of line (010) to (100) was used to define the aspect ratio, since short-rod $CdWO_4$ nanocrystals grew along the normal direction of (100) face and the angle between planes (010) and (100) is very close to the right angle. It is found that the aspect ratios for $CdWO_4$ nanocrystals were varied in a narrow range from 0.67 to 0.74 as particle size increased from 11 to 21 nm.

Particle size can impose great impacts on the lattice parameters. For 11 nm $CdWO_4$, the lattice parameters are $a = 0.5039$ nm, $b = 0.5892$ nm, $c = 0.5105$ nm, and $\beta = 91.71°$, which are all slightly larger than those of the bulk $CdWO_4$ (JCPDS, no. 14-0676). Figure 3 illustrates the particle size dependences of the lattice volume and $\beta$ angle. It is seen that the lattice volume increased monotonically as particle size reduced, which indicates a lattice expansion. Similar phenomena had already been observed in several oxide nanoparticles[12] such as $CaWO_4$, $YPO_4$, rutile $TiO_2$, ZnO, and $\alpha$-$Fe_2O_3$. It is also noted that the lattice expansion is followed by an increase in $\beta$ angle that systematically deviates from the right angle, which indicates

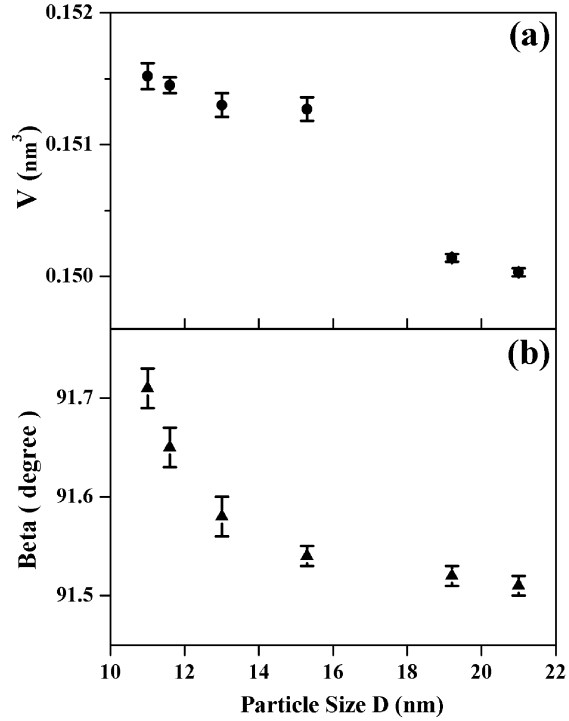


**Figure 3.** Particle size dependences of (a) lattice volume, *V*, and (b) $\beta$ angle of $CdWO_4$ nanocrystals.

the lowered lattice symmetry at small particle sizes. This observation is interesting, since it is contrary to what is observed in many oxide nanoparticles.[12a,b,13] For the latter cases, lattice expansion is popularly accompanied by an enhanced symmetry. The lattice expansion with abnormal symmetry lowering for the monoclinic $CdWO_4$ nanoparticles might be closely related to the interactions of surface exposed layer molecules and the difference between the W−O bond and the Cd−O bond, which will be described below.

It is well-documented that the defect surface chemistry is a highly possible reason for the lattice expansion.[12] As particle size reduces, there will be more atoms exposed on surfaces with lower coordination. These exposed surface atoms will most

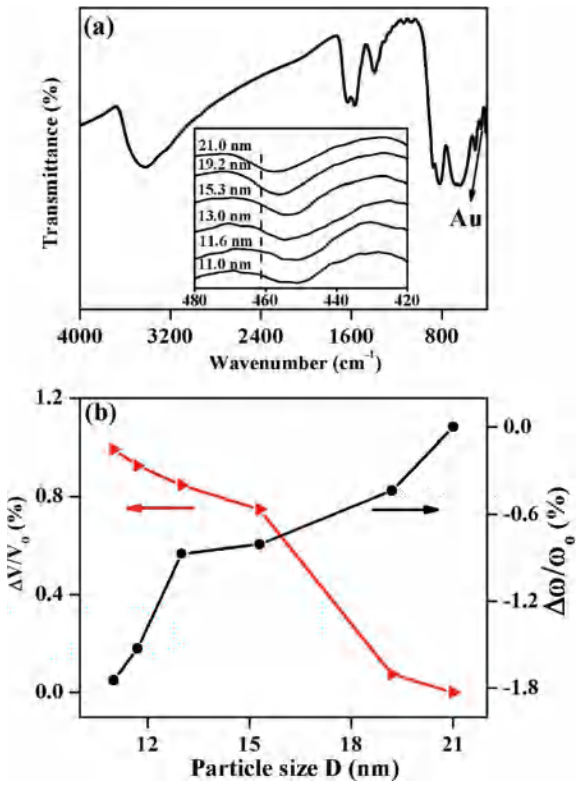


**Figure 4.** (a) IR spectrum of 11 nm $CdWO_4$ and (b) particle size dependences of the relative changes of $A_u$ mode frequency and lattice volume. Inset illustrates the enlarged $A_u$ mode around 455 cm$^{-1}$ for all samples. Relative changes in lattice volume and $A_u$ mode frequency are represented by $\Delta V/V_0 = (V - V_0)/V_0$ and $\Delta\omega/\omega_0 = (\omega_0 - \omega)/\omega_0$, respectively, where $V_0$ and $\omega_0$ denote the lattice volume and $A_u$ mode frequency for 21 nm $CdWO_4$.

likely lead to a significant increase in the numbers of dangling bonds, which could be compensated by absorbing some small molecules like $H_2O$ to form terminal hydration layers, as is confirmed by IR in Figure 4. Because of the polarity and the same tropism of $H_2O$ molecules, surface defect dipoles are expected to be perpendicular to the outer surface of each $CdWO_4$ nanocrystal. The roughly parallel array of surface dipoles would repel each other and result in a larger equilibrium lattice constant than that for the bulk,[13] which explains the apparent lattice expansion for $CdWO_4$ nanocrystals.

Concerning the lowered lattice symmetry, the anisotropic nature of the monoclinic $CdWO_4$ should be taken into account. XRD Rietveld refinements showed that, as the particle size reduced from 21 to 11 nm, both the *b* and *c*-axes became elongated by 0.36% and 0.47%, respectively, which compares to only a 0.12% increase for the *a*-axis. Therefore, the lowered lattice symmetry for $CdWO_4$ nanocrystals is associated with an anisotropic lattice expansion that is likely originated from the variation of the Cd−O bond length in the presence of hard $W-O_6$ octahedra. Since the lattice expansion is equivalent to the "negative pressure", the nature for the lowered lattice symmetry could be acknowledged by comparison with the structural evolution of bulk $CdWO_4$ under high pressure. Lacomba-Perales et al.[7e] studied the pressure dependence of bulk $CdWO_4$ lattice parameters by ab initio total-energy and lattice-dynamics calculations and found anisotropic lattice contraction with increasing pressure in which the Cd−O bond length decreases faster with pressure than the W−O bond length. Consequently, the different chemical nature between W−O and Cd−O bonds can be expected in $CdWO_4$ nanocrystals, which accounts for the lowered lattice symmetry at small particle sizes.

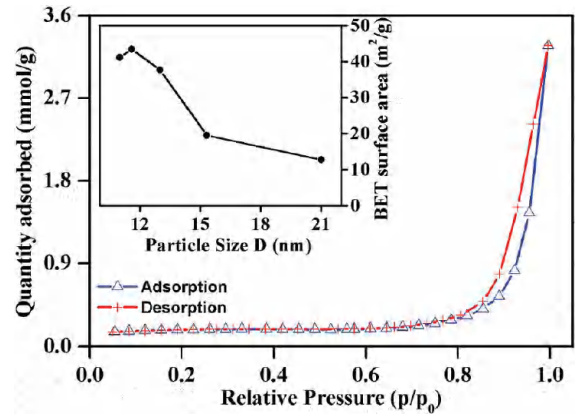


**Figure 5.** Representative nitrogen desorption/adsorption isotherms for 21 nm $CdWO_4$. Inset illustrates the relationship between specific surface area and particle size of $CdWO_4$ nanoparticles.

**3.2. Surface Chemistry and Vibrational Properties of the Size-Controlled Monoclinic $CdWO_4$ Nanophases.** The relationship between particle size and specific surface area of the as-prepared $CdWO_4$ nanocrystals was investigated based on the nitrogen adsorption and desorption isotherm curves. Shown in Figure 5 are the representative adsorption/desorption isotherms for 21 nm $CdWO_4$. Type III isotherm with a type $H_3$ hysteresis loop is observed according to the Brunauer−Deming−Deming−Teller classification.[14] Inset of Figure 5 illustrates the particle size dependence of the BET surface area. It is seen that the BET surface area increased markedly as particle size reduced from 21 to 11 nm.

Large surface area allows surface modifications by chemical species. The chemical species absorbed on surfaces of $CdWO_4$ nanocrystals were examined by FT-IR spectra. Figure 4a shows a typical infrared spectrum for 11 nm $CdWO_4$, and the spectra of other sample are illustrated in the Supporting Information. It is clear that a large amount of absorbed water and hydroxyl groups coexisted on nanostructure surfaces. The broad absorption band centered at 3428 cm$^{-1}$ is attributed to the vibration of H−O bonds for surface hydration layers, and the weak absorption located at 1633 cm$^{-1}$ is associated with the deformation vibration of H−O−H bonds of the water molecules.[15] Two strong bands centered at about 1395 and 1568 cm$^{-1}$ correspond to the symmetrical and asymmetrical vibrations of the carboxylate groups, respectively. Two weak bands detected at 1061 and 1139 cm$^{-1}$ characterized the C−O stretching vibrations of the citric species,[6] which indicates the presence of the citrate capping on $CdWO_4$ nanostructures.

A set of bands below 1000 cm$^{-1}$ in Figure 4a is characteristic of the vibrations of W−O bonds. $CdWO_4$ is thermodynamically stable in a wolframite structure of $C_{2h}^4$ symmetry (space group, *P2/c*). According to the group theory, 33 vibration modes can be expected: $\Gamma = 8A_g + 10B_g + 7A_u + 8B_u$, where $A_u$ and $B_u$ modes are infrared active.[16] $B_u$ mode for asymmetrical and symmetrical stretching vibrations of the short W−O bond in the $WO_4^{2-}$ group is represented by two sharp bands at 823 and 876 cm$^{-1}$ (Figure 4a), while the bands at 679 and 639 cm$^{-1}$ are assigned to the asymmetrical stretching vibrations of the W−O−W bond in the $WO_4^{2-}$ group, respectively. The sharp bands observed at 503, 442, and 407 cm$^{-1}$ are assigned to the in-plane deformation of the $WO_4^{2-}$ group.[17]

As illustrated in the inset of Figure 4a, the $A_u$ mode associated with the deformation vibration of the $WO_4^{2-}$ group shifted toward lower wavenumbers with particle size reduction. To get into the cause for this observation, the relationship between $A_u$

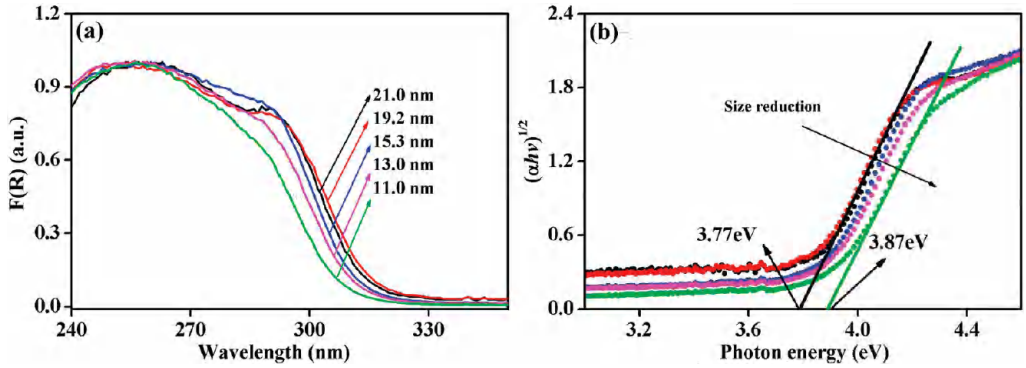


**Figure 6.** (a) UV−visible diffuse reflectance spectra and (b) energy dependence of $(\alpha h\nu)^{1/2}$ for $CdWO_4$ nanocrystals at different particle sizes.

mode frequency change and lattice expansion was first addressed. According to the literature, lattice expansion can give rise to the weakened force constants between pairs of ions, and thus, red shift for the absorption bands can be expected for small sizes like other nanoparticles[12a,b,e] of $CaWO_4$, $YPO_4$, or $\alpha$-$Fe_2O_3$. Figure 4b shows the relative changes in lattice volume and $A_u$ mode frequency as a function of particle size. It is clear that the lattice volume increased while the phonon frequency of $A_u$ mode decreased monotonically. This could be associated with a "polaron" effect in $CdWO_4$ nanocrystals, since the lowering of lattice symmetry is followed by a large red shift of phonon frequency.[6,18] Therefore, lattice expansion and "polaron" effect could be the dominant factors for the red shift of the $A_u$ vibration mode.

**3.3. Electronic Structures of the Size-Controlled Monoclinic $CdWO_4$ Nanophases.** Electronic structures for $CdWO_4$ nanoparticles were measured by diffuse reflectance spectroscopy at room temperature. As demonstrated in Figure 6a, $CdWO_4$ nanocrystals showed an intense band-to-band absorption in the UV region, which is originated from the absorption of the allowed transitions $^1A_{1g} - {}^1T_{1u}$ in the $(WO_6)^{6-}$ complex.[19] Since the particle sizes (>11 nm) of all $CdWO_4$ nanocrystals are much larger than the exciton radius of approximately 4 nm for $CdWO_4$,[19b,c] the optical absorption edge of an idealized parabolic band bulk semiconductor with allowed transitions can be fit using the Tauc equation:[20]

$$\alpha h\nu = K(h\nu - E_g)^{1/n}$$

where $\alpha$ is the absorption coefficient, $K$ is the characteristic constant of semiconductors, $h\nu$ and $E_g$ are photon energy and optical band gap energy, respectively, and $n$ equals $^1/_2$ because $CdWO_4$ is an indirect gap semiconductor.[8,21] The $E_g$ values were thus determined by extrapolation of the linear portion of the $(\alpha h\nu)^n$ curve versus the photon energy $h\nu$ to $(\alpha h\nu)^n = 0$. As illustrated in Figure 6b, the band gap for $CdWO_4$ nanoparticles slightly shifted from 3.77 to 3.87 eV with particle size reduction from 21 to 11 nm. It is well-known that the transition $^1A_{1g} - {}^1T_{1u}$ is electric dipole allowed from the valence band to the conduction band.[19] The slight blue shift in the transition energy for $^1A_{1g} - {}^1T_{1u}$ indicates a broadened band gap, a common feature for bulk semiconductor nanocrystals,[22] which could be related to the surface band bending[23] due to the surface structural modifications of highly concentrated hydroxyls and citric-related groups.

Figure 7 shows the photoluminescence spectra measured at room temperature for $CdWO_4$ nanocrystals of different particle sizes. It is seen that under 290 nm excitation, all $CdWO_4$ nanocrystals gave a broad blue-green emission around 475 nm, which is attributed to the charge-transfer transition between the O 2p orbital and the empty d orbital of the central $W^{6+}$ of $WO_6$ octahedra or to the self-trapped exciton at a $WO_6^{6-}$ oxyanion complex.[24] PL intensity increased to show a maximum as particle size became larger to 21 nm. It is known that several factors such as particle size,[12a] morphology,[25] crystallinity,[26] or surface modification[27] can be responsible for the PL intensity variations. Concerning the morphological impacts, aspect ratio is important in controlling the exciton transport rate as reported for other systems such as silica nanostructures[25g] and CdSe nanocrystals.[25h] Nevertheless, as mentioned above, $CdWO_4$ nanocrystals are all in a similar spindly short-rod shape, showing an aspect ratio varied in a narrow range from 0.67 to 0.74 as the particle size varied from 11 to 21 nm. Therefore, morphological changes might not be the predominant factor for the PL intensity variations. Alternatively, surface hydration layers could be a possible reason, since as for almost all oxide nanoparticles, particle size reduction usually leads to a significant increase in the amounts of surface absorbed water. The increased number of $OH^-$ groups of surface absorbed water might act as the luminescent quencher.[27a] As a consequence, PL intensity for $CdWO_4$ nanocrystals was expected to be relatively weak.

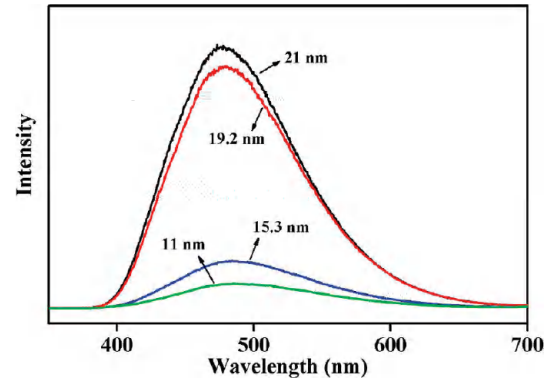


**Figure 7.** Photoluminescence spectra of $CdWO_4$ nanocrystals at given particle sizes under the measurement conditions: solid-state samples, 290 nm excitation, and room temperature.

PL intensity can also be affected by the ligands of the citric species that are absorbed on surfaces, because the citric species could interact with the surface dangling bonds to reduce the numbers of trap sites for nonradiative recombination. In this case, the photoluminescence quantum efficiency could be significantly enhanced,[27c] which is different from what one expects for larger particle sizes of $CdWO_4$ nanoparticles because of the lower concentration of surface citric species. Therefore, there may exist other factors for the increased PL intensity at larger particle sizes (Figure 7). Crystallinity is investigated as

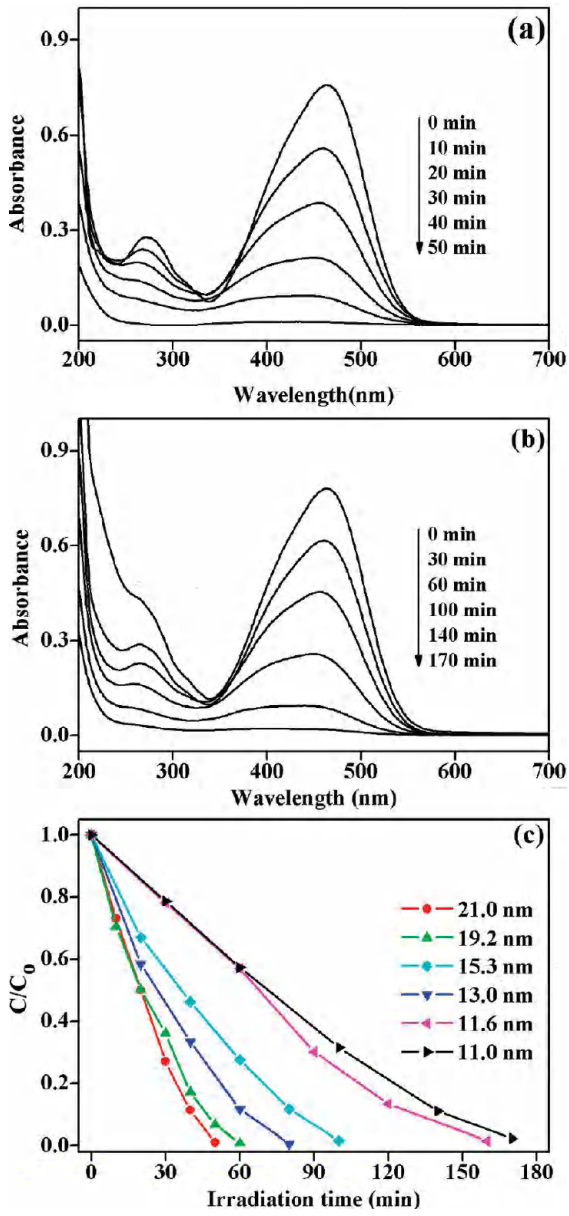


**Figure 8.** Time-dependent absorption spectra of MO solution in the presence of (a) 21 nm $CdWO_4$ and (b) 11 nm $CdWO_4$ under UV light irradiation; (c) photocatalytic activities of $CdWO_4$ nanostructures at different particle sizes.

a possible reason. It is general that the crystallinity increase can result in an enhanced emission intensity.[26] As confirmed by TEM measurement, the crystallinity was much improved with increasing the particle size. The significantly increased emission intensity for larger particle size (Figure 7) indicates the impacts of crystallinity on PL intensity. Therefore, in comparison with other two factors such as particle size and surface modification, crystallinity could play a dominant role.

**3.4. Photocatalytic Activity of the Size-Controlled Monoclinic $CdWO_4$ Nanophases.** Sample characterizations above indicate that lattice structure, band gap, lattice vibration, and photoluminescence of $CdWO_4$ nanocrystals can be systematically controlled by particle size, which expects to give particle size dependence of the properties for technological uses. As an example, the photocatalytic activities of $CdWO_4$ nanoparticles were preliminarily studied. MO molecules were explored as the probe for the photocatalytic activity examination. Figure 8a and b illustrates the time-dependent absorption spectra of MO aqueous solutions during the UV light irradiation in the presence of 11 and 21 nm $CdWO_4$. For both nanostructures, the maximum absorption of the MO solution gradually decreased with prolonging the irradiation time. In the presence of 21 nm $CdWO_4$, MO solution was completely degraded after irradiation for 50 min, while for 11 nm $CdWO_4$, the irradiation time had to last for 170 min to completely remove the MO molecules. Figure 8c shows the normalized absorbance changes of all solutions with irradiation time under UV light. It is clear that with increasing the particle size, photocatalytic activity of $CdWO_4$ nanocrystals became better, among which 21 nm $CdWO_4$ shows the optimum activity.

To understand the variation of photocatalytic activity of $CdWO_4$ nanocrystals, several factors such as electronic structure, surface property, morphology, and crystallinity have to be addressed. Among these factors, the broadened band gap energy is considered as a most likely reason,[29] since it would enhance the redox potentials of the photogenerated electrons and holes. As stated above, the band gap energy for $CdWO_4$ nanocrystals slightly shifted toward the higher energy by only 0.1 eV as particle size reduced from 21 to 11 nm (Figure 6). As a result, the slightly shifted band gap seems not applicable for the present work, since the photocatalytic activity for the as-prepared $CdWO_4$ nanocrystals tended to decrease with particle size reduction.

With regards to the morphology, it is reported that semiconductors of different morphology can exhibit quite different photocatalytic activity.[30] Mclaren et al. investigated the photocatalytic activity of different morphology of ZnO and found that hexagonal platelike particles displayed 5 times higher activity than the rod-shaped particles in photocatalytic degradation of methylene blue.[31] In the present work, the morphological effect on photocatalytic activity can be insignificant, since all $CdWO_4$ nanocrystals had almost the same morphology with roughly the same aspect ratios.

Another important factor could be from either specific surface area or surface modifications. With regards to the surface modification, the surface hydroxyl groups bound to the surfaces may promote the photodegradation process, since much more reactive surface HO• species can be produced and the electron−hole recombination can be hindered.[32] According to the IR analysis, all $CdWO_4$ nanocrystals are terminated by surface hydration layers and citric acid species (Supporting Information), and their relevant contents increased with particle size reduction. Hence, photocatalytic activity is expected to enhance with particle size reduction. However, this expectation is somehow inconsistent with what we observed in $CdWO_4$ nanocrystals. Therefore, there should be other factors that govern the photocatalytic activity.

It is well-documented that the surface area of semiconductors has a great influence on the photocatalytic activity and in some cases can be a dominant factor.[33] For nanocrystals of large surface area, the ratio of the surface charge carrier transfer rate to the electron−hole recombination rate can be greatly improved, resulting in highly concentrated surface active sites and a higher photonic efficiency.[34] Based on this consideration, photocatalytic activity should be enhanced with increasing the surface area. As shown in the inset of Figure 5, the surface area of $CdWO_4$ nanocrystals increased with particle size reduction. Comparing to 15.3 nm $CdWO_4$, the activity for 13 nm $CdWO_4$ became significantly improved (Figure 8c). At this point, surface area seems to be the main factor that influences the photocatalytic activity. However, when we have an overall look at all $CdWO_4$ nanocrystals, it is found that the photocatalytic activity for

$CdWO_4$ nanocrystals enhanced with increasing the reaction temperature regardless of the variations of surface area. Therefore, surface area is also excluded as a possible cause for the photocatalytic activity. The last possible factor could be the crystallinity of $CdWO_4$ nanocrystals. For instance, Amano et al. have found that crystallization of $Bi_2WO_6$ leads to an increase in absorbed photon and photocatalytic reaction efficiency.[3b] Based on the above systematic sample characterization, it is clear that the crystallinity of $CdWO_4$ nanocrystals is extremely enhanced with increasing reaction temperature, which is in accordance with the order of photocatalytic activity of the as-prepared $CdWO_4$ nanocrystals (Figure 8c). Highly crystallized 21 nm $CdWO_4$ displayed activity about 3 times higher than 11 nm $CdWO_4$ (of a relatively low crystallinity) in photodegradation of MO solution. Therefore, crystallinity may dominate the photocatalytic activity of $CdWO_4$ nanostructures. This conclusion is further confirmed by the above photoluminescence: the enhancement of photoluminescence as a result of crystallinity means the delayed recombination of exciton so that electron or hole can be effectively transported for oxidation of methyl orange in water.

## 4. Conclusions

$CdWO_4$ nanocrystals of controlled particle sizes were synthesized by hydrothermal method. When varying the reaction temperature from 220 to 160 °C, the particle size of $CdWO_4$ nanocrystals decreased from 21 to 11 nm. With particle size reduction, there existed a lattice expansion as followed by a lowered lattice symmetry, broadened band gap, and red shift of the $A_u$ vibration mode. Photocatalytic activity of $CdWO_4$ nanocrystals of controlled particle sizes was evaluated by UV-light photodegradation of methyl orange. $CdWO_4$ nanoparticles with particle size of 21 nm showed an excellent photocatalytic activity, which is more than 3 times higher than 11 nm $CdWO_4$. This observation was explained in terms of the crystallinity that varied with the particle sizes of $CdWO_4$ nanostructures. Further work will be highly necessary to understand the contradictory factors of high crystallinity and small sizes for semiconductor nanoparticles that will lead to excellent photocatalytic activity for technological uses.

**Acknowledgment.** This work was financially supported by NSFC (contract nos. 50972143, 20773132, 20771101, and 20831004), National Basic Research Program of China (nos. 2007CB613301 and 2009CB939801), Directional program (KJCXZ-YW-MO5) and Knowledge Innovation Program of the Chinese Academy of Sciences, and FJIRSM key program (no. SZD-07004-3).

**Supporting Information Available:** FT-IR spectra of the as-prepared $CdWO_4$ nanocrystals. This material is available free of charge via the Internet at http://pubs.acs.org.

## References and Notes

(1) (a) Matthews, R. W. *Water Res.* **1991**, *25*, 1169. (b) Sharma, A.; Rao, P.; Mathur, R. P.; Ameta, S. C. A. *J. Photochem. Photobiol. A: Chem.* **1995**, *86*, 197. (c) Sakthivel, S.; Neppolian, B.; Shankar, M. V.; Arabindoo, B.; Palanichamy, M.; Murugesan, V. *Sol. Energy Mater. Sol. Cells* **2003**, *77*, 65. (d) Linsebigler, A. L.; Lu, G. Q.; Yates, J. T. *Chem. Rev.* **1995**, *95*, 735. (e) Thompson, T. L.; Yates, J. T. *Chem. Rev.* **2006**, *106*, 4428.

(2) Pardeshi, S. K.; Patil, A. B. *J. Mol. Catal. A: Chem.* **2009**, *308*, 32.

(3) (a) Ikeda, S.; Sugiyama, N.; Murakami, S.; Kominami, H.; Kera, Y.; Noguchi, H.; Uosaki, K.; Torimoto, T.; Ohtani, B. *Phys. Chem. Chem. Phys.* **2003**, *5*, 778. (b) Amano, F.; Yamakata, A.; Nogami, K.; Osawa, M.; Ohtani, B. *J. Am. Chem. Soc.* **2008**, *130*, 17650. (c) Honda, K.; Fujishima, A. *Nature* **1972**, *238*, 37. (d) Sopyan, I.; Watanabe, M.; Murasawa, S.; Hashimoto, K.; Fujishima, A. *J. Photochem. Photobiol. A: Chem.* **1996**, *98*, 79.

(4) (a) Roselin, L. S.; Rajarajeswari, G. R.; Selvin, R.; Sadasivam, V.; Sivasankar, B.; Rengaraj, K. *Sol. Energy* **2002**, *73*, 281. (b) Height, M. J.; Pratsinis, S. E.; Mekasuwandumrong, O.; Praserthdam, P. *Appl. Catal. B: Environ.* **2006**, *63*, 305. (c) Ohtani, B.; Bowman, R. M.; Colombo, D. P.; Kominami, H.; Noguchi, H.; Uosaki, K. *Chem. Lett.* **1998**, *27*, 579. (d) Dodd, A.; McKinley, A.; Saunders, M.; Tsuzuki, T. *Nanotechnology* **2006**, *17*, 692.

(5) (a) Yang, J. L.; An, S. J.; Park, W. I.; Yi, G.; Choi, W. *Adv. Mater.* **2004**, *16*, 1661. (b) Cao, L. X.; Spiess, F. J.; Huang, A.; Suib, S. L.; Obee, T. N.; Hay, S. O.; Freihaut, J. D. *J. Phys. Chem. B* **1999**, *103*, 2912. (c) Li, L. P.; Liu, J. J.; Su, Y. G.; Li, G. S.; Chen, X. B.; Qiu, X. Q.; Yan, T. J. *Nanotechnology* **2009**, *20*, 155706.

(6) Su, Y. G.; Li, G. S.; Xue, Y. F.; Li, L. P. *J. Phys. Chem. C* **2007**, *111*, 6684.

(7) (a) Chen, W. B.; Inagawa, Y.; Omatsu, T.; Tateda, M.; Takeuchi, N.; Usuki, Y. *Opt. Commun.* **2001**, *194*, 401. (b) Lecoq, P.; Dafinei, I.; Auffray, E.; Scheegans, M.; Korzhik, M. V.; Missetvitch, O. V.; Pavlenko, V. B.; Fedorov, A. A.; Annenkov, A. N.; Kostylev, V. L.; Ligun, V. D. *Instrum. Methods Phys. Res. A* **1995**, *365*, 291. (c) Ishii, M.; Kobayashi, M. *Prog. Cryst. Growth Charact. Mater.* **1992**, *23*, 245. (d) Fagherazzi, G.; Pernicone, N. *J. Catal.* **1970**, *16*, 321. (e) Lacomba-Perales, R.; Errandonea, D.; Martinez-Garcia, D.; Rodríguez-Hernández, P.; Radescu, S.; Mujica, A.; Muñoz, A.; Chervin, J. C.; Polian, A. *Phys. Rev. B* **2009**, *79*, 094105. (f) Lotem, H.; Burshtein, Z. *J. Opt. Lett.* **1987**, *12*, 561. (g) Pustovarov, V. A.; Krymov, A. L.; Shulgin, B. V. *Rev. Sci. Instrum.* **1992**, *63*, 3521. (h) Greskovich, C. D.; Cusano, D.; Hoffman, D. R. J. *Am. Ceram. Soc. Bull.* **1992**, *71*, 1120.

(8) Ye, D.; Li, D. Z.; Zhang, W. J.; Sun, M.; Hu, Y.; Zhang, Y. F.; Fu, X. Z. *J. Phys. Chem. C* **2008**, *112*, 17351.

(9) (a) Wang, Y. G.; Ma, J. F.; Tao, J. T.; Zhu, X. Y.; Zhou, J.; Zhao, Z. Q.; Xie, L. J.; Tian, H. *Ceram. Int.* **2007**, *33*, 1125. (b) Liao, H. W.; Wang, Y. F.; Liu, X. M.; Li, Y. D.; Qian, Y. T. *Chem. Mater.* **2000**, *12*, 2819. (c) Wang, Y. G.; Ma, J. F.; Tao, J. T.; Zhu, X. Y.; Zhou, J.; Zhao, Z. Q.; Xie, L. J.; Tian, H. *J. Am. Ceram. Soc.* **2006**, *89*, 2980.

(10) (a) Chung, K. T. *Mutat. Res.* **1983**, *114*, 269. (b) Chung, K. T.; Stevens, S. E.; Cernigla, C. E. *Crit. Rev. Microbiol.* **1992**, *18*, 175. (c) Ökte, A. N.; Yílmaz, Ö. *Appl. Catal. A: Gen.* **2009**, *354*, 132.

(11) Chen, D.; Shen, G. Z.; Tang, K. B.; Zheng, H. G.; Qian, Y. Q. *Mater. Res. Bull.* **2003**, *38*, 1783.

(12) (a) Li, L. P.; Su, Y. G.; Li, G. S. *Appl. Phys. Lett.* **2007**, *90*, 054105. (b) Liu, Q.; Su, Y. G.; Yu, H. S.; Han, W. *J. Rare Earths* **2008**, *26*, 495. (c) Li, G. S.; Boerio-Goates, J.; Woodfield, B. F.; Li, L. P. *Appl. Phys. Lett.* **2004**, *85*, 13. (d) Li, L. P.; Qiu, X. Q.; Li, G. S. *Appl. Phys. Lett.* **2005**, *87*, 124101. (e) Lu, L.; Li, L. P.; Wang, X. J.; Li, G. S. *J. Phys. Chem. B* **2005**, *109*, 17151.

(13) Ayyub, P.; Palkar, V. R.; Chattopadhyay, S.; Multani, M. *Phys. Rev. B* **1995**, *51*, 6135.

(14) (a) Gregg, S. J.; Sing, K. S. W. *Adsorption, Surface Area and Porosity*, 2nd ed.; Academic Press: London, 1982, p 4. (b) Sing, K. S. W.; Everett, D. H.; Haul, R. A. W.; Moscou, L.; Pierotti, R. A.; Rouquerol, J.; Siemieniewska, T. *Pure Appl. Chem.* **1985**, *57*, 603.

(15) (a) Hu, W. B.; Li, L. P.; Li, G. S.; Meng, J.; Tong, W. M. *J. Phys. Chem. C* **2009**, *113*, 16996. (b) Li, G. S.; Li, L. P.; Boerio-Goates, J.; Woodfield, B. F. *J. Am. Chem. Soc.* **2005**, *127*, 8659.

(16) Gabrusenoks, J.; Veispals, A.; von Czarnowski, A.; Meiwes-Broer, K. H. *Electrochim. Acta* **2001**, *46*, 2229.

(17) Daturi, M.; Busca, G.; Borel, M. M.; Leclaire, A.; Piaggio, P. *J. Phys. Chem. B* **1997**, *101*, 4358.

(18) Kim, K. H.; Gu, J. Y.; Choi, H. S.; Park, G. W.; Noh, T. W. *Phys. Rev. Lett.* **1996**, *77*, 1877.

(19) (a) Mikhailika, V. B.; Kraus, H.; Miller, G.; Mykhaylyk, M. S.; Wahl, D. *J. Appl. Phys.* **2005**, *97*, 083523. (b) Vielhauer, S.; Babin, V.; De Grazia, M.; Feldbach, E.; Kirm, M.; Nagirnyi, V.; Vasil'ev, A. *Phys. Solid State* **2008**, *50*, 1789. (c) Fedorov, N.; Nagirnyi, V.; Vasil'ev, A.; Belsky, A.; Carre, B.; Feldbach, E.; Gaudin, J.; Geoffroy, G.; Guizard, S.; De Grazia, M.; Kirm, M.; Martin, P.; Merdji, H.; Petite, G. *J. Phys. IV* **2006**, *138*, 251.

(20) Huxter, V. M.; Mirkovic, T.; Nair, P. S.; Scholes, G. D. *Adv. Mater.* **2008**, *20*, 2439.

(21) (a) Kortuem, G. *Reflectance Spectroscopy: Principles, Methods, Applications*; Springer-Verlag: Berlin, Germany, 1969. (b) Hu, W. B.; Li, L. P.; Li, G. S.; Tang, C. L.; Sun, L. *Cryst. Growth Des.* **2009**, *9*, 3676.

(22) (a) Lin, K. F.; Cheng, H. M.; Hsu, H. C.; Lin, L. J.; Hsieh, W. F. *Chem. Phys. Lett.* **2005**, *409*, 208. (b) Yoffe, A. D. *Adv. Phys.* **2001**, *50*, 1.

(23) Chen, W.; Qi, D. C.; Gao, X. Y.; Wee, A. T. S. *Prog. Surf. Sci.* **2009**, *84*, 279.

(24) Rzhevskaya, O. V.; Spasskii, D. A.; Kolobanov, V. N.; Mikhaĭlin, V. V.; Nagornaya, L. L.; Tupitsina, I. A.; Zadneprovskiĭ, B. I. *Opt. Spectrosc.* **2008**, *104*, 366.

(25) (a) Luo, Y. S.; Zhang, W. D.; Dai, X. J.; Yang, Y.; Fu, S. Y. *J. Phys. Chem. C* **2009**, *113*, 4856. (b) Nakazaki, A. Y.; Fujita, K.; Tanaka,

K.; Uchino, T. *J. Phys. Chem. C* **2008**, *112*, 10878. (c) Sun, F.; Guo, Y. P.; Song, W. B.; Zhao, J. Z.; Tang, L. Q.; Wang, Z. C. *J. Cryst. Growth* **2007**, *304*, 425. (d) Wang, D. B.; Song, C. X.; Hue, Z. S. *Cryst. Res. Technol.* **2008**, *43*, 55. (e) Kwak, M. G.; Park, J. H.; Shon, S. H. *Solid State Commun.* **2004**, *130*, 199. (f) Dong, F. Q.; Wu, Q. S. *Appl. Phys. A: Mater. Sci. Process.* **2008**, *91*, 161. (g) Wang, Y.; Zhang, R.; Frauenheim, T.; Niehaus, T. A. *J. Phys. Chem. C* **2009**, *113*, 12935. (h) Califano, M.; Bester, G.; Zunger, A. *Nano Lett.* **2003**, *3*, 1197.

(26) (a) Yu, M.; Lin, L.; Fang, J. *Chem. Mater.* **2005**, *17*, 1783. (b) Pang, M. L.; Lin, J.; Yu, M. *J. Solid State Chem.* **2004**, *177*, 2237. (c) Yu, M.; Lin, J.; Fu, J.; Zhang, H. J.; Han, Y. C. *J. Mater. Chem.* **2003**, *13*, 1413. (d) Yu, M.; Wang, Z.; Fu, J.; Wang, S.; Zhang, H. J.; Han, Y. C. *Chem. Mater.* **2002**, *14*, 2224. (e) Yu, M.; Lin, J.; Zhou, Y. H.; Wang, S. B.; Zhang, H. J. *J. Mater. Chem.* **2002**, *12*, 86. (f) Lin, J.; Sänger, D. U.; Mennig, M.; Bärner, K. *Thin Solid Films* **2000**, *360*, 39.

(27) (a) Haas, Y.; Stein, G. *Chem. Phys. Lett.* **1972**, *15*, 12. (b) Di, W. H.; Wang, X. J.; Chen, B. J.; Lu, S. Z.; Zhao, X. X. *J. Phys. Chem. B* **2005**, *109*, 13154. (c) Konishi, M.; Isobe, T.; Senna, M. *J. Lumin.* **2001**, *93*, 1.

(28) Sun, M.; Li, D. Z.; Zhang, W. J.; Chen, Z. X.; Huang, H. J.; Li, W. J.; He, Y. H.; Fu, X. Z. *J. Phys. Chem. C* **2009**, *113*, 14916.

(29) Cao, L. X.; Spiess, F. J.; Huang, A. M.; Suib, S. L.; Obee, T. N.; Hay, S. O.; Freihaut, J. D. *J. Phys. Chem. B* **1999**, *103*, 2912.

(30) Li, D.; Haneda, H. *Chemosphere* **2003**, *51*, 129.

(31) Mclaren, A.; Valdes-Solis, T.; Li., G. Q.; Tsang, S. C. *J. Am. Chem. Soc.* **2009**, *131*, 12540.

(32) Carp, O.; Huisman, C. L.; Reller, A. *Prog. Solid State Chem.* **2004**, *32*, 33.

(33) (a) Ohko, Y.; Fujishima, A.; Hashimoto, K. *J. Phys. Chem. B* **1998**, *102*, 1724. (b) Gu, D. E.; Lu, Y.; Yang, B. C.; Hu, Y. D. *Chem. Commun.* **2008**, *21*, 2453. (c) Soni, S. S.; Henderson, M. J.; Bardeau, J. F.; Gibaud, A. *Adv. Mater.* **2008**, *20*, 1493. (d) Song, X. F.; Gao, L. *J. Phys. Chem. C* **2007**, *111*, 8180.

(34) Zhang, Z. B.; Wang, C. C.; Zakaria, R.; Ying, J. Y. *J. Phys. Chem. B* **1998**, *102*, 10871.

JP910284U